JAMES | Journal of Advances in Modeling Earth Systems®

RESEARCH ARTICLE
10.1029/2024MS004695

A Robust Constraint on the Response of Convective Mass Fluxes to Warming

Andrew I. L. Williams[1] and **Nadir Jeevanjee**[2]

[1]Program in Atmospheric and Oceanic Sciences, Princeton University, Princeton, NJ, USA, [2]Geophysical Fluid Dynamics Lab, Princeton, NJ, USA

Key Points:

- Convective mass fluxes robustly decrease with warming, at around $3-5\%K^{-1}$, when viewed in temperature coordinates
- The weakening in temperature coordinates is explained by the stabilization of the lapse rate under warming
- The scaling of Held and Soden (2006), https://doi.org/10.1175/jcli3990.1 does not capture simulated mass flux changes with warming

Supporting Information:

Supporting Information may be found in the online version of this article.

Correspondence to:

A. I. L. Williams,
andrew.williams@princeton.edu

Citation:

Williams, A. I. L., & Jeevanjee, N. (2025). A robust constraint on the response of convective mass fluxes to warming. *Journal of Advances in Modeling Earth Systems*, *17*, e2024MS004695. https://doi.org/10.1029/2024MS004695

Received 5 SEP 2024
Accepted 9 MAR 2025

Abstract A fundamental quantity in tropical dynamics is the "convective mass flux," which measures the rate at which mass is transported upwards per unit area in convective updrafts. Convective mass flux encodes information about the frequency and intensity of thunderstorms, and has been linked to the strength of the large-scale tropical circulation. Changes in convective mass flux under warming are an important, but uncertain, aspect of climate change. Here we build off recent work linking changes in mass flux to the clear-sky energy budget to show that convective mass fluxes decrease along isotherms at around 3%–5% K^{-1} under warming. We show that this constraint holds throughout the free-troposphere and across a hierarchy of models; from idealized radiative-convective equilibrium simulations to CMIP6 models. This decrease in convective mass flux with warming is driven by a stabilization of the lapse rate and can be captured with a simple analytical model. We also revisit previous work by Held and Soden (2006), https://doi.org/10.1175/jcli3990.1, who proposed a scaling for changes in the convective mass flux with warming. We show that the Held and Soden scaling does not capture inter-model spread in cloud-base mass flux changes under warming, and that their original verification was likely coincidental. Our work provides a quantitative constraint on changes in convective mass flux throughout the troposphere which can be derived from first principles, and which is verified across a hierarchy of models.

Plain Language Summary In the tropics, the primary way that mass is transported vertically is through deep convective updrafts. The rate at which mass is transported upwards, per unit area, is termed the "convective mass flux." In the literature, there are two main perspectives on how convective mass flux will respond to warming; one focusing on the clear-sky energy budget and the other focusing on moisture fluxes between the boundary layer and the free-troposphere (Held & Soden, 2006, https://doi.org/10.1175/jcli3990.1). Here we test these two perspectives using an ensemble of high-resolution models which can explicitly simulate deep convective updrafts. We find that the predictions based off of the clear-sky energy budget are robust, while the Held and Soden scaling does not accurately capture changes in mass fluxes with warming. We further argue that simple moist physics can be used to predict the relative magnitude of changes in convective mass flux if temperature is used as a vertical coordinate (rather than height or pressure).

1. Introduction

On a flight through the tropics, if you look out the window of an airplane you will likely see broad areas of dry descending air driven by radiative and evaporative cooling alongside narrow, moist regions of intense ascent driven by towering cumulonimbus clouds (Malkus & Riehl, 1964). These convective updrafts are associated with the overwhelming majority of ascent in the tropics, and hence the rate at which mass is transported upwards in the tropics (per unit area) is often termed the "convective mass flux" (M_c). Convective mass flux is defined as

$$M_c = \rho \sigma_{up} w_{up}, \tag{1}$$

where ρ is the density of air, w_{up} is the convective updraft velocity and σ_{up} is the fraction of the domain covered by convective updrafts.

Simulated M_c profiles, diagnosed using Equation 1, are shown in Figure 1. We use data from the Radiative–Convective Equilibrium Model Intercomparison Project (RCEMIP, Wing et al. (2018)); we will discuss radiative-convective equilibrium in more detail later on. Consistent with observational estimates of M_c, the

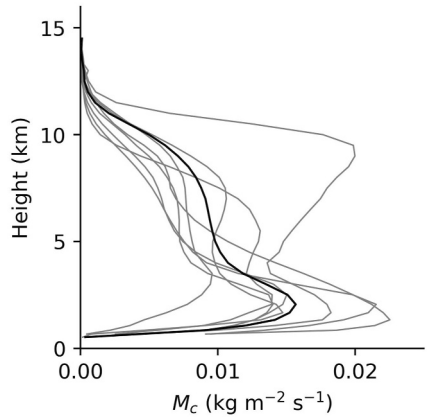

Figure 1. *Vertical structure of M_c in RCEMIP models.* Gray lines show vertical profiles of convective mass flux (M_c) across RCEMIP models (Wing et al. (2018), Methods) for the simulations with 295 K sea-surface temperature. Black lines indicate the ensemble mean M_c.

profiles generally exhibit an increase in mass-flux at low levels, peak a few kilometers above the surface and then become small near the tropopause (Savazzi et al., 2021; Schiro et al., 2018).

When considering how M_c changes with warming, studies often cite the seminal work of Held and Soden (2006) (hereafter HS06). HS06, approximating the work of Betts (1998), suggested that the convective latent heat flux at cloud-base should balance the latent heat release from precipitation (in the global-/tropical-mean). This was written heuristically as

$$P = \left(M_c\, q_v^*\right)|_{LCL}. \tag{2}$$

Here P is the precipitation, q_v^* is the saturation specific humidity, and we have denoted cloud-base (the interface between the boundary layer and the free-troposphere) as the lifted condensation level (LCL). We note that Equation 2 differs from Betts' original formulation by neglecting cloud-base relative humidity, as will be important in Section 7.

From Equation 2, HS06 then argued that convective mass fluxes at cloud-base should *decrease* with warming due to the mismatch between the rapid increase of boundary layer saturation specific humidity and the slower increase in precipitation under warming.

The HS06 scaling (embodied in Equation 2) is frequently cited in the literature as the physical basis for a weakening of M_c under warming (Watanabe et al., 2023), including the IPCC's Fifth Assessment Report (Collins et al., 2013). Many studies have also used Equation 2 to *diagnose* changes in mass flux with warming in models and observations (He et al., 2024; Shrestha & Soden, 2023; Vecchi & Soden, 2007). However, despite its prominence, the validity of the HS06 scaling has been called into question (Jeevanjee, 2022; Schneider et al., 2010). In particular, Jeevanjee (2022, hereafter J22) found that Equation 2 poorly captures the behavior of cloud-base M_c under warming in two cloud-resolving models and that cloud-base M_c can sometimes *increase* with warming despite a decrease in $P/q_v^*|_{LCL}$. This tension motivates further study into the validity of Equation 2, and to understand why it may not be a robust constraint on cloud-base M_c changes under warming.

An alternative approach for studying the response of M_c to warming is to use the paradigm of radiative-convective equilibrium (RCE) (Jeevanjee, 2022; Jenney et al., 2020). RCE describes a state where convective heating is balanced by radiative and evaporative cooling (Manabe & Strickler, 1964). This balance holds by definition in the RCEMIP simulations (Figure 1), but is also a good approximation for the real tropical atmosphere on large scales (Jakob et al., 2019). In the tropical-/domain-mean, RCE demands that the upwards mass flux in convection (M_c) be balanced by descent in clear, subsiding air as a result of radiative and evaporative cooling (M_{sub}). The subsidence mass flux is defined as $M_{sub} = \rho\sigma_{sub}w_{sub}$, with $M_c + M_{sub} = 0$ in RCE.

Utilizing the aforementioned balance between M_c and M_{sub}, and assuming weak temperature gradient balance (Sobel et al., 2001), M_c can thus be written as

$$M_c = -\rho\sigma_{sub}w_{sub} = -\rho\sigma_{sub}\frac{\mathcal{H}_{rad} + \mathcal{H}_{evap}}{\Gamma_d - \Gamma}. \tag{3}$$

Here $\mathcal{H}_{rad}$ and $\mathcal{H}_{evap}$ are the radiative and evaporative cooling rates, both negative and in units of K/s, Γ_d is the dry lapse rate and Γ is the true lapse rate (Jeevanjee, 2022; Jenney et al., 2020). The denominator, $(\Gamma_d - \Gamma)$, is positive due to the presence of moisture, which causes the true lapse rate to be more stable than the dry lapse rate. Previous work has argued that (all else equal) the clear-sky subsidence velocity should weaken with warming due to the stabilizing impact of warming on the lapse rate (Held & Soden, 2006; Knutson & Manabe, 1995; Larson et al., 1999). By Equation 3, this argument also implies a weakening of convective mass fluxes with warming.

A weakness of the preceding argument is that while the denominator of Equation 3 is thermodynamically constrained to increase under warming and drive a reduction of M_c, changes in radiative cooling in particular are not similarly constrained. To tackle this issue, J22 showed that Equation 3 could be rewritten as

$$M_c = \frac{\sigma_{sub}}{\alpha} \frac{-\partial_T F}{g\left(\frac{1}{\Gamma} - \frac{1}{\Gamma_d}\right)}. \quad (4)$$

Here g is the acceleration due to gravity, $-\partial_T F$ is the radiative flux divergence in temperature coordinates (replacing the radiative cooling in Equation 3) and α is a vertically resolved, horizontally averaged "conversion efficiency," which measures the ratio of net latent heating to gross latent heating. Note that J22 assumed $\sigma_{sub} \approx 1$, which holds when convection is explicitly resolved but not in GCMs (Figure S1 in Supporting Information S1). The benefit of this expression over Equation 3 is that, to a good approximation, $-\partial_T F$ is only a function of the *local* atmospheric temperature (Jeevanjee & Romps, 2018). Hence, if we use temperature as our vertical coordinate (as opposed to height or pressure), then the profile of $-\partial_T F$ is now *insensitive* to changes in surface temperature (Jeevanjee & Romps, 2018; Stauffer & Wing, 2022).

In contrast to insensitivity of $-\partial_T F(T)$ to changes in surface temperature, the "inverse stability" factor, $(1/\Gamma - 1/\Gamma_d)^{-1}$, decreases quite rapidly with surface warming, even at a fixed isotherm (J22). Hence, barring large changes in α (and σ_{sub}, Figure S1 in Supporting Information S1) with warming, we expect that the decreases in $(1/\Gamma - 1/\Gamma_d)^{-1}$ with warming will dominate, and thus that *convective mass fluxes should decrease along isotherms with surface warming*. This is the crucial prediction arrived at by J22, and which was verified in two cloud resolving models and using parameterized subgrid convective mass flux output from GFDL's CM4 model. Whether this prediction holds up across a larger ensemble of models and whether it can also constrain the *magnitude* of M_c changes remains to be seen.

Given the promising results of J22 and the longstanding tensions in the literature regarding the HS06 scaling, our primary goal here is to test the robustness of each of these constraints using an ensemble of cloud resolving simulations conducted as part of the Radiative-Convective Equilibrium Model Intercomparison Project (RCEMIP; Wing et al. (2018)). We begin by focusing on the J22 prediction, and show that it does indeed hold up across RCEMIP models; that is, convective mass fluxes decrease with surface warming when viewed along isotherms. We then build upon the work of J22 by showing that, when considered at a given isotherm, not only is the *sign* of M_c changes constrained, but also their relative *magnitude* (in $\%K^{-1}$). Specifically, we find that fractional changes in M_c with warming are approximately 3%–5% K^{-1} along isotherms. To explain this, we develop a simple analytical expression for the expected change in M_c in response to surface warming, assuming that microphysical changes are small and that the lapse rate is moist adiabatic. We also confirm that this constraint on mass flux changes also holds in CMIP6 models. We end by showing that the HS06 scaling does not capture M_c changes with warming in cloud-resolving models, in contrast to our theory, and that the original verification of the HS06 scaling is neither physically justified nor robust across models.

2. Methods

2.1. RCEMIP Simulations

The RCEMIP Phase One protocol and main results are described in Wing et al. (2018, 2020), respectively. We use the "RCE_small" cloud-resolving simulations, which have a domain of $\sim$ 100x100km^2, $\sim$74 vertical levels and $\sim$1 km horizontal resolution. Note that the "RCE_small" simulations we use do not exhibit convective self-aggregation. Each simulation is run with constant, horizontally uniform SSTs at three different levels: 295, 300 and 305 K. The models are each integrated for 100 days and we use the last 25 days of each simulation, during which instantaneous 3D output is available at six-hour intervals. Fractional changes (units of $\%$ K^{-1}) are calculated as $\frac{100}{\Delta T}\ln(\Phi_{\text{pert}}/\Phi_{\text{ctrl}})$, where ΔT is the surface temperature change and Φ is the quantity of interest in the perturbed (e.g., 305 K) and control (e.g., 295 K) simulations, following O'Gorman and Muller (2010).

We used all cloud-resolving models for which the required data was available. The two exceptions to this are the UKMO model and the ICON model. The UKMO model submitted multiple variants and so we only take a single variant (UKMOi-vn11.1-CASIM) so as not to over-represent a single model, but our conclusions are unchanged if we include all four UKMO variants. We also discard the two ICON cloud-resolving models as their M_c profiles exhibit roughly twice as much temporal variability as other models (not shown), suggesting that the ICON models require more than the $\sim$100 3D snapshots available in order to robustly characterize their convective mass flux

profiles. The eight models we used are: dam, UKMOi-vn11.1-CASIM, WRF_COL_CRM, SAM_CRM, SCALE, MESONH, UCLA-CRM and CM1.

2.2. Calculation of M_c in RCEMIP

To calculate the convective mass flux (M_c) in the simulations with explicit convection, we first identify cloudy updrafts as those grid cells which have cloud condensate mixing ratios (liquid + ice) greater than 10^{-5} kg kg^{-1} and upwards vertical velocities greater than 1 ms^{-1} (all results are similar if we instead use a 0.25 ms^{-1} threshold). Convective mass fluxes are then defined at each level (averaging along constant isotherms or constant heights, as needed) as $M_c \equiv \rho w_{up} \sigma_{up}$ (kg m^{-2} s^{-1}) where w_{up} is the vertical velocity (w) conditionally averaged (with area weighting, where appropriate) over all cloudy updrafts, and σ_{up} is the fractional area occupied by cloudy updrafts compared to the total area of the domain (roughly $\sim 100 \times 100$ km^2 in RCEMIP and extending ± 20°N in the global simulations). Air density (ρ) is calculated from the ideal gas law using the local temperatures and pressures.

2.3. CMIP6 Simulations

We use daily temperature, pressure, geopotential height and vertical pressure velocity (ω), along with monthly mean subgrid convective mass fluxes, from the AMIP and AMIP-p4K experiments conducted as part of CMIP6. Not all models archived daily mean ω and/or subgrid convective mass flux, and those which did sometimes did not provide the data at high enough vertical resolution to do the interpolation to temperature coordinates, so we used slightly different subset of models in panels (a) and (b) of Figure 3. For panels (a) and (b) of Figure 3 we used GFDL-CM4, IPSL-CM6A-LR, MRI-ESM2-0, BCC-CSM2-MR, MIROC6. For panels (c) and (d) we used NorESM2-LM, CanESM5, GFDL-CM4, MIROC6 and GISS-E2-1-G. We analyze the tropics, defined as the region from ± 20°N.

There is an ambiguity in what quantity to take as the "convective mass flux" when analyzing these CMIP simulations because there is a distinction between "subgrid" and "resolved" mass flux in coarse-resolution models. This is analogous to the distinction between "convective" and "large-scale" precipitation in GCMs. Many CMIP6 models outputted monthly mean subgrid convective mass flux, M_c^{subgrid}, which is indicative of the subgrid convective heating, and this output has been used in previous studies (e.g., Chadwick et al. (2013)). However, the subgrid convective mass flux is only one component of the total mass flux in the model, and is not necessarily indicative of the large-scale, resolved mass flux in the models. So, to complement our analysis of subgrid mass fluxes, we also calculated a "large-scale" mass flux, $M_{up} = (-1/g)\sigma_{up}\omega_{up}$ (equivalent to Equation 1, by hydrostatic balance), by conditionally sampling daily mean upwards vertical velocities in the tropics and calculating an area fraction based off of that. Daily mean vertical velocities were interpolated to temperature coordinates before conditionally sampling. We note that this form of large-scale mass flux is similar in spirit to that employed by Schneider et al. (2010).

When interpolating data to temperature (T) coordinates, we first need to identify a range of free-tropospheric temperatures over which T varies monotonically. We take the upper boundary of this region to be the highest level above 300 hPa which still has temperature decreasing with height. The lower boundary is taken to be the 850 hPa level if there are no low-level temperature inversions, otherwise the pressure of the lower boundary is $\min(p_{inv}, 850hPa)$, where p_{inv} is the pressure of the low-level temperature inversion (e.g., the trade inversion). After selecting this region, we then interpolate all variables onto a uniform temperature grid (300–180 K in 2.5 K increments).

When using temperature coordinates, one must also be careful with behavior at the lower boundary. For example, the 240 K isotherm is defined at every point in the tropics (± 20°N) in the AMIP control run, but the 280 K isotherm is not always defined at every tropical grid-cell because of cold intrusions from the extratropics or the influence of orography. Hence, when plotting changes with warming in temperature coordinates, we first cut off the profiles at the lowest level where not every tropical (± 20°N) grid-cell is defined at that temperature. This is done to avoid aliasing changes in the "amount" of the tropics which is defined along an isotherm into our %K^{-1} values.

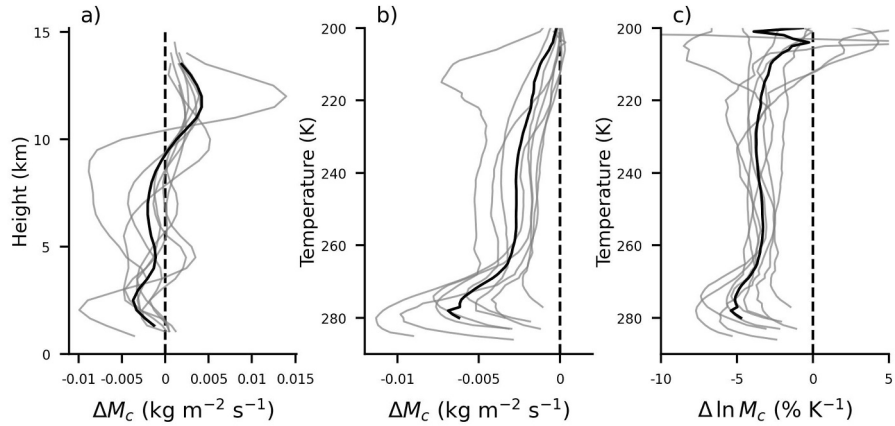

Figure 2. *Changes in M_c with warming are robustly negative, when considered along isotherms*. Panel (a) Changes in M_c between the RCEMIP simulations with 305 and 295 K SST, plotted in z-coordinates. Individual models are plotted in gray and the ensemble mean is plotted in black at every level where at least 7 models out of 8 have data. (b) As in panel (a), but plotted using temperature as the vertical coordinate. (c) As in panel (b) but showing the fractional changes in M_c per degree of warming (% K^{-1}). We are focused on free-tropospheric mass fluxes and so for clarity the profiles are cut off below cloud base (defined as the low-level maximum in cloud fraction) and above the cold point tropopause.

3. Response of M_c Profiles to Warming in RCEMIP

To begin with, we will use the RCEMIP experiments to test the prediction recently proposed by Jeevanjee (2022), that M_c should decrease along isotherms with surface warming. In Figure 2, we plot changes in convective mass flux profiles (ΔM_c) between the 305 and 295 K experiments in RCEMIP. Figure 2a shows the changes plotted in height coordinates (profiles cut off below cloud-base and above the cold point tropopause) and demonstrates a substantial scatter across models. For example, whereas in the upper-troposphere (above 10 km) all models exhibit an increase in M_c with warming, below 10 km there is little agreement on the sign of the change. Additionally, one can see that several of the models exhibit weak changes in cloud-base M_c and some models even simulate an *increase* in cloud-base M_c, contrary what is predicted by the HS06 scaling (we will return to this later on).

In Figure 2b, we plot the same ΔM_c profiles from RCEMIP, but now using temperature as a vertical coordinate, motivated by Equation 4. In line with the prediction of J22 we find that ΔM_c is consistently negative and that convective mass fluxes decrease along almost all isotherms with surface warming. That ΔM_c is negative along isotherms with surface warming was shown previously by J22 for two cloud resolving models, and Figure 2b confirms that this result holds across a much wider range of cloud-resolving models. Furthermore, the prediction of a decrease of M_c along isotherms was arrived at by assuming that stability-induced changes in M_c dominate over changes associated with conversion efficiency (α). That ΔM_c is robustly negative in Figure 2b further bolsters this assumption and highlights the importance of lapse-rate changes.

In the very upper troposphere, a couple of models exhibit small, positive changes in M_c under warming (Figure 2b), which may indicate that changes in α dominate over lapse-rate changes at this level in these models. However, convective updrafts which reach up to the 200 K isotherm are rare in these simulations and so the positive ΔM_c may potentially be caused by sampling issues due to only having ∼100 3D snapshots per model.

While the decrease of M_c in Figure 2b confirms J22's prediction on the *sign* of ΔM_c, there is still substantial spread across models. Furthermore, the magnitude of ΔM_c is quite different between the upper- and lower-troposphere. One possible cause of this spread is the "baseline" M_c profiles in the 295 K simulation, which differ substantially across models (see Figure 1 and Figure S2 in Supporting Information S1), particularly in the upper-troposphere. To account for this, in Figure 2c we present the same ΔM_c profiles as in Figure 2b, but now normalized by the M_c values in the 295 K simulation (and divided by 10 K to get units of % K^{-1}).

Having done this, in Figure 2c we find that the RCEMIP models simulate a fractional decrease in M_c which is remarkably constrained throughout the free-troposphere (around 3%–5% K^{-1}), particularly between the freezing level ($\approx$ 270K) and the anvil level ($\approx$ 220K). This result is notable both because of the degree of model agreement (the models agree to within a factor of 2 at almost all isotherms, though they diverge in the upper-troposphere) and additionally because the result they agree is on is fairly vertically uniform (in contrast to the changes in Figure 2b). More quantitatively, note that the coefficient of variation, defined as the ensemble standard deviation normalized by the magnitude of the ensemble mean, is 0.5 along the 250 K isotherm in Figure 2b, compared to 0.2 along the 250 K isotherm in Figure 2c. Thus, fractional changes are better constrained than absolute changes compared to the ensemble mean M_c change. This result holds at all isotherms and suggests that a large source of inter-model spread in ΔM_c under warming is due to inter-model spread in base-state M_c profiles, at least in RCEMIP.

4. Importance of Stability for M_c Changes Under Warming

We have just shown that across a diverse ensemble of cloud-resolving models, convective mass fluxes decrease along isotherms with surface warming and that throughout most of the troposphere they do so at a fractional rate of around 3%–5%K^{-1}. This simplicity is remarkable considering that many aspects of the convective response to warming are highly *unconstrained* across the RCEMIP ensemble (Stauffer & Wing, 2022), which suggests that some there may be a basic physical mechanism which underlies these M_c and their robustness across models. This section explores such a possibility.

To begin with, we take the logarithmic derivative of Equation 4, at a fixed isotherm (throughout Sections 4 and 5, all derivatives with respect to T_s are taken along isotherms), with respect to surface temperature:

$$\frac{d\ \ln M_c}{dT_s} = \frac{d\ \ln(1/\Gamma - 1/\Gamma_d)^{-1}}{dT_s} + \frac{d\ \ln(-\partial_T F)}{dT_s} + \frac{d\ \ln(1/\alpha)}{dT_s} + \frac{d\ \ln(\sigma_{sub})}{dT_s}. \tag{5}$$

As explained earlier, we expect that changes in $-\partial_T F$ with surface warming should be small when $-\partial_T F$ is taken at a fixed isotherm. We confirm this in Figure S3 in Supporting Information S1, which shows that fractional changes in $-\partial_T F$ across models are small throughout most of the troposphere. We will also neglect the third term, which measures contributions from microphysical changes. We do not have a theoretical justification for this (and RCEMIP outputs are insufficient to calculate it explicitly) but we note that J22 found that changes in α with warming were negligible in their FV3 simulations (their Figure A1c). We also find that fractional changes in σ_{sub} are small in both RCEMIP and GCM simulations (Figure S1 in Supporting Information S1), so neglect the final term. This leaves us with:

$$\frac{d\ \ln M_c}{dT_s} \approx \frac{d\ \ln(1/\Gamma - 1/\Gamma_d)^{-1}}{dT_s} = \left(\frac{1}{1 - \frac{\Gamma}{\Gamma_d}}\right) \frac{d\ \ln \Gamma}{dT_s}. \tag{6}$$

This equation encapsulates the heuristic argument presented in the introduction, namely that the stabilizing impact of warming on the lapse rate should cause a decrease in convective mass fluxes.

To confirm that changes in the lapse rate are indeed the dominant factor driving the decrease of M_c along isotherms with surface warming, in Figure 3a we plot the changes in convective mass flux (same as in Figure 2c), and in Figure 3b we plot the fractional changes in $(1/\Gamma - 1/\Gamma_d)^{-1}$. The disagreement between panels (a) and (b) is a measure of the validity of Equation 6 and the uncertainty associated with diagnosing small M_c values in the upper-troposphere. While the agreement is not perfect, changes in the inverse stability still capture the magnitude of changes in M_c (around 3%–5%K^{-1}). There is generally less inter-model spread in $(1/\Gamma - 1/\Gamma_d)^{-1}$ changes than M_c at a given isotherm (e.g., around 260 K), which we interpret as additional spread from changes in $\partial_T F$ and α.

The simulated profiles in Figures 3a and 3b differ most in the upper troposphere, particularly above the $\approx$220K isotherm. Changes in $\partial_T F$ are of the wrong sign to explain this discrepancy (Figure S3 in Supporting Information S1), which would imply a large fractional increase in α. However, we note that Equation 4 was derived using the "zero-buoyancy plume" assumption (Singh & O'Gorman, 2013) and thus does not account for convective transport of sensible heat (Equation 10 of J22). This is a good approximation, but can break down in

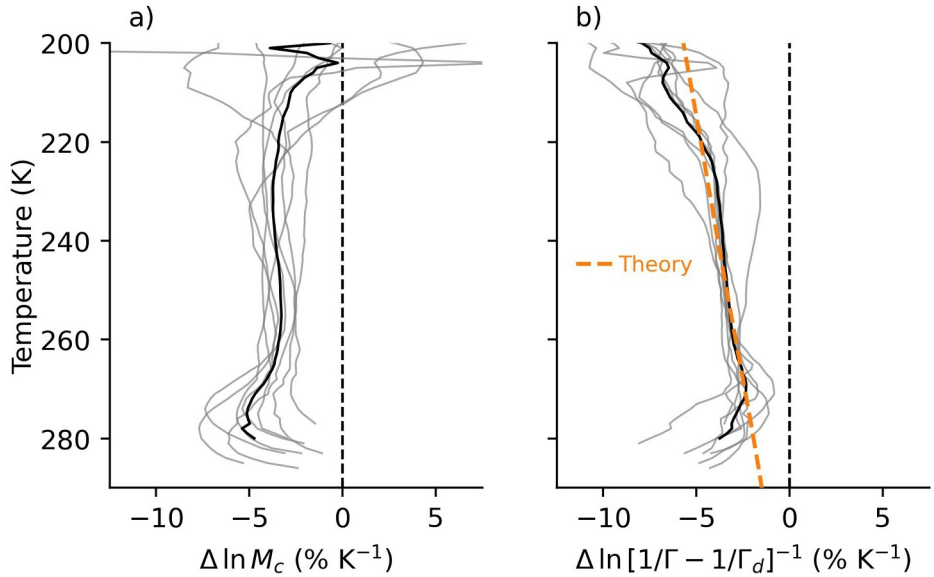

Figure 3. *Changes in M_c (along isotherms) are driven by lapse rate changes.* Panel (a) is the same as Figure 1c. Panel (b) shows the contribution to fractional changes in M_c which comes from lapse-rate changes alone, in RCEMIP models (gray). A moist adiabatic prediction for the lapse-rate contribution is shown in the orange dashed line (evaluated at an SST of 300 K).

the upper troposphere (see Figure 11 of Grabowski et al. (2000) and discussion in Mapes (2001)). Hence the neglect of sensible heat flux changes may also contribute to the disagreement between simulated profiles in Figures 3a and 3b in the upper troposphere.

5. An Analytical Model for M_c Changes Under Warming

Overall, it seems that if we are to understand the origins of the robust, fractional weakening of convective mass fluxes in temperature coordinates, we need to think more deeply about the lapse rate and its changes with warming. To do so, we begin by replacing Γ in Equation 6 with the expression for a non-dilute moist adiabat, Γ_m, which we write as $\Gamma_m = \Gamma_d \left(\frac{1+\beta q_v^*}{1+\gamma q_v^*}\right)$ where $\beta = \frac{L}{R_v T}$ and $\gamma = \frac{L^2}{c_p R_v T^2}$ are both constant along an isotherm. This yields:

$$\frac{d\ln M_c}{dT_s} \approx -\left(\frac{1}{1+\beta q_v^*}\right)\frac{d\ln q_v^*}{dT_s}. \tag{7}$$

Because q_v^* decreases rapidly as a parcel moves up through the atmosphere, the term in parentheses rapidly approaches unity and is of secondary importance compared to the fractional derivative of q_v^* along an isotherm.

It is worth taking a moment to think about what this means. Equation 7 tells us that fractional changes in M_c with warming are controlled by fractional changes in q_v^*, evaluated on a fixed isotherm. At first glance this may be counter-intuitive given the strong dependence of q_v^* on temperature, but the insight here is that even on a fixed isotherm, T, $q_v^*(T)$ will increase with surface warming because the *pressure* associated with that isotherm is decreasing as it rises vertically (Bony et al., 2016; Romps, 2016). Mathematically, because $q_v^*(T,p) = \frac{\epsilon e^*(T)}{p}$, we can write the fractional derivative of $q_v^*(T)$ with respect to surface temperature changes as

$$\frac{d\ln q_v^*}{dT_s} = -\frac{d\ln p}{dT_s}, \tag{8}$$

which shows the essential role played by changes in *pressure* along an isotherm.

We now seek an expression for how pressure (at a given isotherm) responds to surface temperature changes. To do this we use hydrostatic balance and the ideal gas law:

$$\frac{dp}{p} = -\frac{g}{R_a T}\, dz = \frac{g}{R_a T}\, \frac{dT}{\Gamma_{\text{bulk}}} \tag{9}$$

where we have introduced the "bulk lapse rate" between the surface and tropopause, $\Gamma_{\text{bulk}} = -\frac{dT}{dz} = -(T_s - T_{tp})/(z_s - z_{tp})$, which allows us to transform from height to temperature coordinates. Here T_{tp} is the tropopause temperature, z_{tp} is the tropopause height and T_s and z_s are the same but for the surface. We treat Γ_{bulk} as constant in height within a given climate, but it is allowed to change between climates (as T_s and/or z_{tp} change). Now we can integrate Equation 9 between the surface and the pressure level with temperature T to get:

$$p(T) = p_s \left(\frac{T}{T_s}\right)^{g/R_a\Gamma_{\text{bulk}}} \tag{10}$$

we now derive an expression for Γ_{bulk}. Given that T_s is known and z_s is zero at the surface, if we assume the tropopause temperature stays constant in response to surface temperature changes (in line with the FAT/FiTT hypothesis; Hartmann and Larson (2002); Seeley et al. (2019); McKim et al. (2024)), then all that is needed is an expression for how the tropopause height, z_{tp}, depends on T_s. We obtain this by equating the surface moist static energy with the saturation moist static energy at the tropopause, and assuming the surface relative humidity to be unity (following Koll et al. (2023)),

$$z_{tp} \approx \frac{1}{g}\left[c_p(T_s - T_{tp}) + L_v q_s^*\right], \tag{11}$$

where q_s^* is the surface saturation specific humidity and we have neglected the saturation specific humidity at the tropopause. Using these approximations, we can write the logarithmic derivative of pressure (along an isotherm) with respect to surface temperatures changes as:

$$\frac{d\ln p}{dT_s} = \underbrace{-\frac{g}{R_a T_s \Gamma_{\text{bulk}}}}_{\substack{\text{Constant } \Gamma_{\text{bulk}} \\ \approx 2\%\ \text{K}^{-1}}} + \underbrace{\frac{L q_s^*}{R_a (T_s - T_{tp})}\left(\frac{L}{R_v T_s^2} - \frac{1}{T_s - T_{tp}}\right)\ln\left(\frac{T}{T_s}\right)}_{\text{Contribution from changes in } \Gamma_{\text{bulk}} \text{ with warming}}. \tag{12}$$

The first term on the right hand side of Equation 12 arises through taking the logarithmic derivative of Equation 10 with respect to surface temperature changes, at constant Γ_{bulk}, and evaluates to around $2\%\text{K}^{-1}$ (note this term is also derived in the appendix of Romps (2014)). This first term is constant throughout the troposphere, as we use a constant Γ_{bulk} to characterize the tropical lapse rate. However, Γ_{bulk} can change with warming as a result of changes in T_s and z_{tp}, via Equation 11. These changes in Γ_{bulk} with warming introduce an additional term to Equation 12, which increases in magnitude as we move up through the atmosphere. The fact that changes in Γ_{bulk} with warming have a larger $\%\text{K}^{-1}$ impact on pressures in the upper-troposphere than the lower-troposphere arises due to the non-linear relationship between pressure and temperature in Equation 10.

Together, Equations 7, 8, 10 and 12 form a fully analytical model for the contribution to changes in M_c which arise due to simple, moist-adiabatic changes in the lapse rate.

In Figure 3b we plot our theoretical prediction for the lapse rate contribution (dashed orange line) on top of the RCEMIP results. The analytical model is evaluated at a surface temperature of 300 K, as the RCEMIP results are taken as a difference between 305 and 295 K. We find that the analytical prediction sits neatly in the range of the RCEMIP results and is very accurate throughout most of the free-troposphere. The main exceptions to this are in the lower- and upper-regions of the troposphere, where the lapse rate is known to depart from simple, moist adiabatic behavior (Singh & O'Gorman, 2013; Zhou & Xie, 2019). Notably, in the upper-troposphere the RCEMIP models exhibit lapse rate changes which are systematically more stabilizing than the moist adiabatic

prediction. This is in contrast to what would be expected if entrainment (which our analytical model does not account for) was the cause of the discrepancy; entrainment generally causes upper-tropospheric warming which is *weaker* than implied by non-dilute changes (Miyawaki et al., 2020). To check the impact of entrainment, we numerically integrated the "entraining adiabat" from Romps (2016) (with $a = 0.2$) and compared it to a non-dilute adiabat. When these profiles were plugged into Equation 6 we found that entrainment weakened the lapse rate contribution by about 0.5% K^{-1}.

We hypothesize this anomalous stabilization is due to the fact that RCEMIP models have an ozone profile which is fixed in pressure, and so in the 305 K simulation the upper-troposphere experiences anomalous shortwave heating from ozone, which stabilizes this region of the atmosphere in addition to the stabilization expected from the moist adiabat. Nevertheless, despite these caveats, we can conclude that it is the stabilization of the lapse rate under warming which drives the decrease of M_c in temperature coordinates, and that these changes in the lapse rate can be understood by considering simple, moist adiabatic physics.

6. Understanding M_c Changes in Height Coordinates

We have shown that our analytical theory successfully captures the ensemble-mean behavior of lapse rate and M_c changes in temperature coordinates (Figure 3). However, as shown in Figure 2a, there is significant inter-model spread in the response of M_c to warming in *height* coordinates. To understand this inter-model spread and relate it to our theory, we now introduce an expression for M_c changes in height coordinates and use it to explain the inter-model spread in Figure 2a.

To arrive at an expression for fractional changes in M_c with warming at a fixed height, z_0, note that the mass flux at a given height can be written as $M_c(T_s, z) = M_c(T_s, T(z, T_s))$. If we then differentiate both sides with respect to T_s at fixed z and use the chain rule, we arrive at,

$$\left.\frac{d\ \ln M_c(z)}{dT_s}\right|_{z_0} = \left.\frac{d\ \ln M_c(T)}{dT_s}\right|_{T(z_0)} - \frac{1}{\Gamma(z_0)} \left.\frac{dT(z)}{dT_s}\right|_{z_0} \left.\frac{d\ \ln M_c(z)}{dz}\right|_{z_0}. \tag{13}$$

Equation 13 tells us that fractional changes in M_c with warming at certain height z_0 are determined by four factors.

1. Fractional changes in $M_c(T)$ with warming along the isotherm $T(z_0)$, $\left.\frac{d\ \ln M_c(T)}{dT_s}\right|_{T(z_0)}$.
2. The lapse rate in the control run, Γ, evaluated at z_0.
3. The amplification of temperature changes with height, $\frac{dT(z)}{dT_s}$, evaluated at z_0.
4. The vertical gradient of $\ln M_c(z)$ in the control climate, $\frac{d\ \ln M_c(z)}{dz}$, evaluated at z_0.

The first term on the right-hand side of Equation 13 is predicted by the analytical theory we developed in the previous section (the orange line in Figure 3b). The second term represents an "upwards shift" of the $M_c(z)$ profile with warming.

Before applying Equation 13 to RCEMIP simulations, lets consider some examples. First, consider the simple case of a M_c profile which is constant in the vertical. In this case the vertical gradient of $M_c(z)$ is zero, and M_c will decrease by $\approx 3 - 5\%K^{-1}$ in height coordinates as well as in temperature coordinates. This situation is illustrated schematically in Figures 4a and 4b.

Second, we can consider the more realistic case of a M_c profile which has a single maximum in the lower troposphere (in the control simulation). Such a profile has $\frac{d\ \ln M_c(z)}{dz} > 0$ below the maximum and $\frac{d\ \ln M_c(z)}{dz} < 0$ above it. In this case the second term in Equation 13 is positive below the maximum and negative above it. This extra term causes further reductions in M_c at heights below the maximum, but *offset* these reductions in M_c at heights above the maximum. In fact, if the gradient in M_c is large enough, the second term may completely overwhelm the $\approx 3 - 5\%K^{-1}$ weakening from the first term and generate *increases* in M_c at heights above the maximum. This situation is illustrated schematically in Figures 4c and 4d. Hence, Equation 13 tells us that changes in M_c at a fixed height can be *either positive or negative* and that this depends on the "shape" of $M_c(z)$ in the control simulation.

With this understanding in hand, we can use Equation 13 to predict changes in M_c at a given height in the RCEMIP simulations. To evaluate Equation 13, we calculate the first term on the right-hand side using our analytical theory for M_c changes in temperature coordinates (Section 5) and assume the amplification of

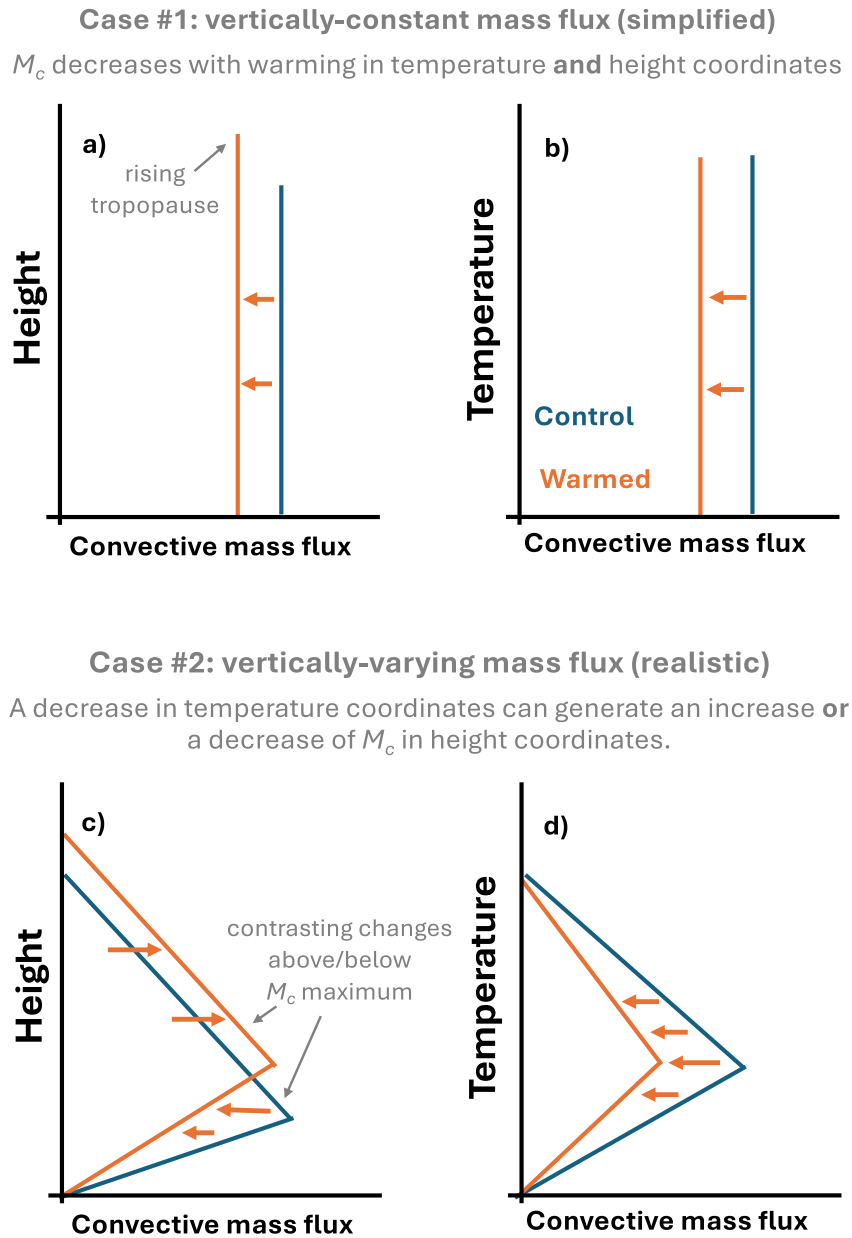

Figure 4. *M_c always decreases in temperature coordinates, but can increase or decrease in height coordinates.* Schematic representation of how M_c changes in temperature coordinates relate to changes in height coordinates. Panels (a) and (b) consider the simple case where M_c is vertically constant, in which case M_c decreases with warming in both coordinate systems. Panels (c) and (d) consider the more realistic case where the profile of M_c has a maximum in the lower troposphere. In this case, M_c still decreases in temperature coordinates, but can either increase or decrease in height coordinates.

temperature changes with height is moist adiabatic. The only additional information we need is knowledge of the $M_c(z)$ and $T(z)$ profiles in the control simulation to calculate the vertical gradient of $\ln M_c(z)$ and $1/\Gamma(z_0)$. Our estimate for M_c changes at fixed height is thus a "true" prediction, as it only requires theoretical inputs and information about the control state.

The result of this procedure is shown in Figure 5, where we have scattered the fractional changes in diagnosed M_c at 5 km against the predicted values using our theory applied to the control simulations. Our theory is able to capture most of the inter-model spread ($r = 0.74$) in M_c changes under warming in RCEMIP (similar skill is found throughout the troposphere; Figure S4 in Supporting Information S1). In particular, our approach is able to

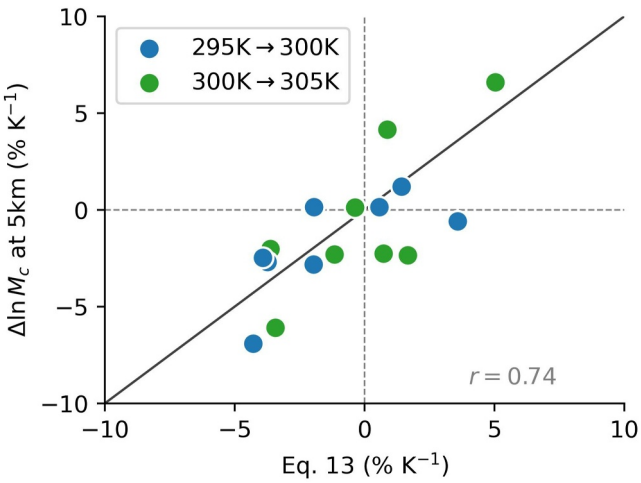

Figure 5. *Our theory captures inter-model spread in M_c changes across RCEMIP.* Fractional changes in M_c at 5 km, diagnosed from RCEMIP simulations, against the changes predicted by Equation 13. The prediction only requires knowledge of the control $M_c(z)$ and $T(z)$ profiles, and the analytical theory in Figure 3b.

capture the fact that changes in M_c with warming at a given height *can be positive or negative*, even if they decrease robustly in temperature coordinates (Figure 2c).

7. Applicability to GCMs With Parameterized Convection

So far we have studied convective mass fluxes and their response to warming in highly idealized RCE simulations. These simulations have the benefit of explicitly resolving deep convection, and thus permitting an unambiguous diagnosis of the convective mass flux by conditionally sampling grid cells. However, these simulations lack many key aspects of Earth's tropics; rotation, large-scale overturning circulations, a diurnal cycle, convectively coupled waves and so on. In this section, we ask whether the theory and insights developed using RCE models with explicit convection, can yield insights into the behavior of fully complexity GCMs with parameterized convection. To do this, we have analyzed a subset of AMIP and AMIP-p4K simulations from CMIP6 (Methods).

The main questions we ask are: Does M_c decrease along isotherms with surface warming? Are fractional changes in M_c similar to those implied by lapse rate changes? Can the lapse rate changes be captured using our simple analytical model?

In Figure 6 we show fractional changes in M_c and the inverse stability contribution in temperature coordinates, where M_c is estimated either using the monthly mean subgrid convective mass flux (top row) or using the "large-scale" M_{up} calculated using daily mean ω (bottom row, Methods). The stability contribution differs between the top and bottom row because the subset of AMIP models used is different (not all models archived daily mean ω and/or subgrid convective mass flux, and those which did sometimes did not provide the data at high enough vertical resolution to do the interpolation to temperature coordinates).

Turning our attention to the top row of Figure 6, we can see that the model-mean subgrid convective mass fluxes decreases with warming at a value of around $5\%\text{K}^{-1}$ throughout the free-troposphere, and that the inverse stability contribution is highly constrained and reasonably well captured by our simple theory. There is more spread in the response of subgrid convective mass fluxes to warming here than in the explicitly diagnosed M_c from the RCEMIP ensemble (Figure 2c); for example, the model range at the 250 K isotherm is $\approx 2\%\text{K}^{-1}$ for RCEMIP but $\approx 6\%\text{K}^{-1}$ for the subgrid mass flux (Figure 6a). We hypothesize that this enhanced spread is driven by changes in the partitioning of subgrid-/resolved-scale precipitation formation under warming. As shown by Held et al. (2007), the partitioning between subgrid-/resolved-scale precipitation can change with warming, and is sensitive to how entrainment is formulated in the convection scheme.

In contrast to the response of subgrid convective mass fluxes, the changes in "large-scale" M_{up} are tightly constrained across the AMIP simulations, with a small spread across the 5 models considered (only $\approx 2\%\text{K}^{-1}$ at the 250 K isotherm). These changes in M_{up} also neatly track the inverse stability contribution shown in Figure 6d. This demonstrates that changes in large-scale mass flux in CMIP6 models are very tightly constrained, a fact which has not been previously noted in the literature. Leveraging the constrained nature of changes in M_{up} to understand the link between mass fluxes and tropical circulation strikes us as a useful avenue for future study.

To summarize, both the subgrid convective mass fluxes and the large-scale M_{up} decrease along isotherms with surface warming, as predicted by theory. These changes with warming are comparable in magnitude to the inverse stability contribution, which is consistent with there being only small changes in $\partial_T F$ and α with warming. The changes in inverse stability themselves are captured reasonably well by our simple analytical model, although the GCM profiles are more stabilizing in the upper troposphere. This could potentially be due to cloud radiative feedbacks, the treatment of ozone, the limitations of our bulk lapse rate assumption or errors introduced by the interpolation to temperature coordinates. Future work is needed to disentangle these different sources of error.

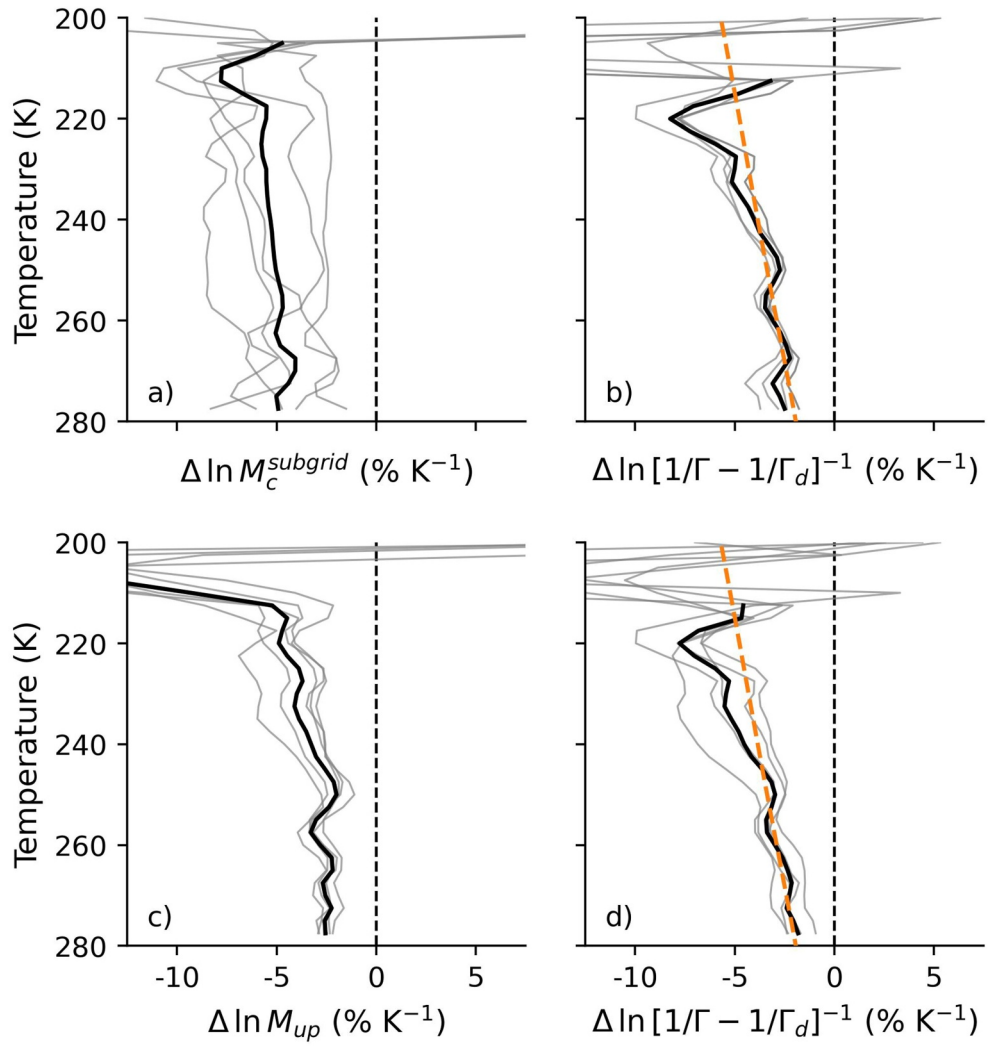

Figure 6. Stabilization of the lapse rate drives M_c weakening in GCMs. Fractional changes in M_c and the inverse stability per degree warming, in temperature coordinates, where M_c is estimated either using the monthly-mean subgrid convective mass flux (a, b) or using the 'large-scale' M_{up} calculated using daily-mean ω (c, d). The stability contribution differs between the top and bottom row because the subset of AMIP models used is different. The dashed orange line in panels (b) and (d) is the same as in Figure 3. The ensemble mean is shown in black at every level where all models agree on the sign of the change.

8. Testing the Held and Soden Scaling in RCEMIP

We have just shown that fractional changes in free-tropospheric M_c with warming are tightly constrained when viewed in temperature coordinates, both in CRMs and GCMs. However, as noted in the introduction, the HS06 scaling (Equation 2) is what is typically cited in the literature as the physical basis for changes in M_c with warming. Here we test whether the HS06 scaling can capture changes in cloud-base M_c with warming across the ensemble of RCEMIP simulations; we also revisit HS06's original verification of Equation 2 and show that it is not robust across GCMs.

In Figure 7a we plot the diagnosed changes in cloud-base convective mass flux against those inferred from the HS06 scaling (Equation 2). We diagnose $q_v^*|_{LCL}$ as the average of q_v over the lowest 5 model levels, as this is characteristic of the boundary layer values and thus of saturated parcels at cloud-base. Cloud-base M_c is estimated by averaging M_c over the lowest 1–2 km.

The HS06 scaling consistently predicts a decrease in cloud-base M_c of around 2%–3%K^{-1}, in line with expectations. However, the models actually *simulate* a wide range of changes in cloud-base M_c. Some simulations

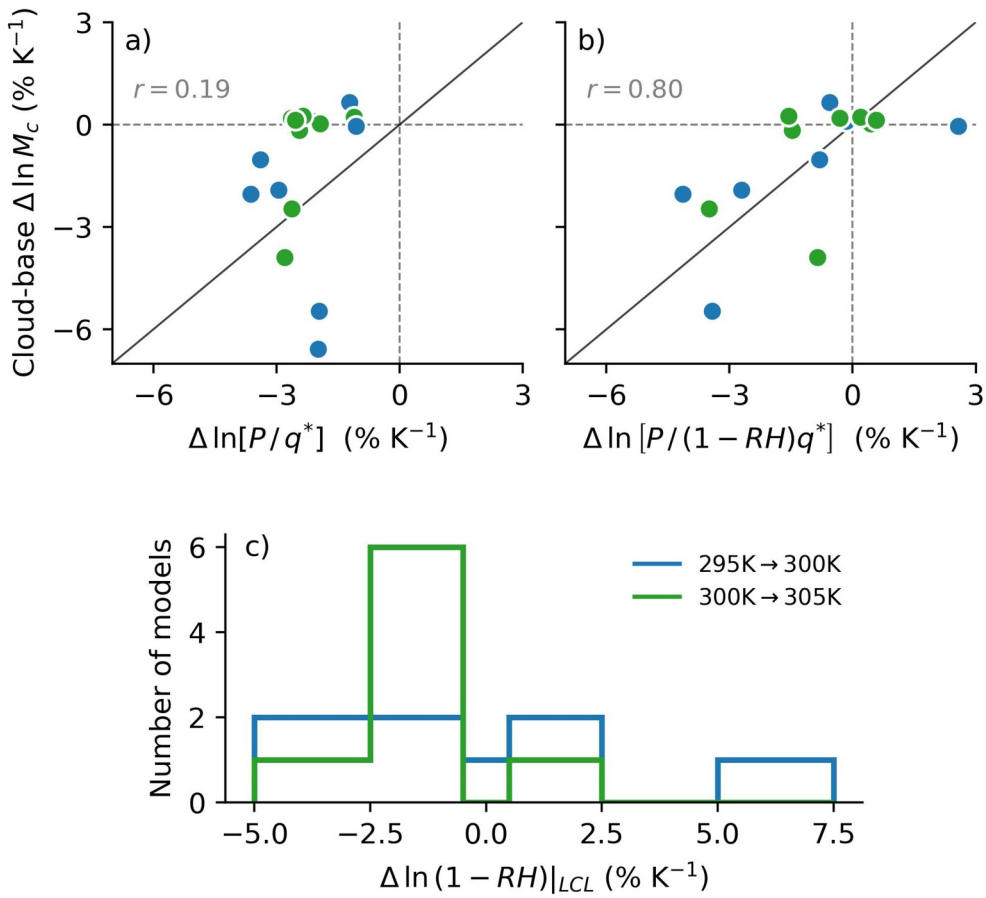

Figure 7. *The HS06 scaling does not capture changes in cloud-base M_c under warming, as it neglects changes in RH_{LCL}.* (a) Fractional changes in cloud-base M_c, directly diagnosed from RCEMIP simulations, against predictions from Equation 2. (b) As in panel (a) but using predictions from Equation 14. (c) Histogram of fractional changes in $(1 - RH)|_{LCL}$ with warming in RCEMIP models.

exhibit decreases of around 6%K^{-1}, while about half of the simulations exhibit negligible (or even positive) changes in cloud-base M_c. Increases in cloud-base M_c with warming can also be seen in Figure 2a, where the profiles are cut off at cloud base. This is consistent with the CRM results of J22, who also showed that the HS06 scaling did not capture the changes in cloud-base M_c.

So, why does the simple reasoning behind Equation 2 fail? Well, the most obvious deficiency of Equation 2 is that it was derived (heuristically) under the explicit assumption that all water vapor lofted above cloud-base both condenses and precipitates to the surface. Hence, Equation 2 neglects factors such as precipitation efficiency and the dilution of moisture via entrainment, both of which are poorly constrained observationally and theoretically. However, it is possible to derive forms of Equation 2 which *do not* make these assumptions, the simplest being:

$$P = \left[M_c (1 - RH)\, q_v^*\right]|_{LCL}. \tag{14}$$

Equation 14 was first derived by Betts (1998) and recently re-derived by J22 (their Appendix C), who termed it "Betts' Rule." Equation 14 is a horizontally averaged water budget; the net flux of water vapor out of the boundary layer (right hand side) must equal the flux of condensed water into the boundary layer *which, neglecting rain re-evaporation in the boundary layer, equals* the precipitation (left hand side). Despite accounting for entrainment, detrainment and non-unit precipitation efficiency, it bears a striking similarity to the HS06 scaling up to an additional factor of $(1 - RH_{LCL})$. This factor accounts for transport of water vapor from the free-troposphere into the boundary layer through subsidence and downdrafts.

Can Equation 14 succeed where Equation 2 did not? In Figure 7b we show the same experiments as in Figure 7a, but now the x-axis shows the prediction for changes in cloud-base M_c *including* the factor of $(1 - RH_{LCL})$ from Equation 14. Both cloud-base M_c and RH_{LCL} are diagnosed as their values averaged over the 1–2 km layer. The relevant relative humidity in Equation 14 is the environmental RH, which we approximate using a domain-average. The improved correlation between simulated and predicted changes in Figure 7b ($r = 0.80$) compared to Figure 7a ($r = 0.19$) shows that Equation 14 is better able to capture the inter-model spread of changes in cloud-base M_c under warming than the HS06 scaling. In contrast to Equation 2, which consistently predicted changes of around 2%–3%K^{-1}, Equation 14 is able to predict a much wider range of changes in cloud-base M_c (including increases with warming), which are more tightly clustered around the 1-to-1 line than those in Figure 7a.

However, although Equation 14 is a more quantitatively accurate model of changes in cloud-base M_c under warming than Equation 2, this skill comes at the cost of requiring changes in RH_{LCL} as an input. Figure 7c shows that changes in $(1 - RH_{LCL})$ with warming can be comparable in size to the fractional changes in $P/q_v^*|_{LCL}$. Furthermore, the sign of changes in $(1 - RH_{LCL})$ is unconstrained across the RCEMIP models. Given that Equation 14 was derived without neglect of entrainment/detrainment and non-unit precipitation efficiency, this suggests that the value of RH_{LCL} must depend on these processes (whose changes under warming are poorly understood). Hence, while Equation 14 is able to capture some of the inter-model spread in cloud-base M_c, it does not provide a strong a priori constraint on these changes as we do not have a theory for changes in RH_{LCL} with warming.

We note that similar concerns apply to vertically integrated forms of the HS06 constraint (Chadwick et al., 2013; Liu et al., 2024). In Figure S7 in Supporting Information S1 we show that vertically averaged M_c also deviates from the HS06 scaling (see further discussion in Text S1 in Supporting Information S1).

An additional complication when using the HS06 scaling or Betts' Rule (Equation 14), is that these constraints apply to mass fluxes at "cloud-base." However, identifying an appropriate cloud-base level is not always straightforward. We discuss this issue further in Appendix A. Given all of these issues, we conclude that the HS06 scaling is not a quantitatively accurate model for changes in cloud-base M_c because it neglects changes in RH_{LCL} with warming.

8.1. How Does This Square With HS06's Own "Verification" of P = Mq?

At this point, one may ask "Didn't HS06 verify Equation 2 in their paper?" In HS06 (their Figure 3b), they indeed "verified" Equation 2 using global-mean, subgrid M_c at 500 hPa in a single GCM (GFDL-CM2.1); we reproduce this result—using their data—in Figure B1a of Appendix B. However, this approach is not consistent with the atmospheric water budget on which Equation 14 (and hence Equation 2) rests. As noted previously, the water budget requires that the net fluxes of water vapor and condensed water be equal and opposite across any level. At cloud-base, the upwards flux of condensed water is negligible, and thus the net vapor flux out of the boundary layer balances the precipitation. However, if we use a higher level, like 500 hPa, then we would have to take account of the upwards flux of condensed water in updrafts, and the fact that the downwards flux of condensed water no longer equals the precipitation. Hence, it is physically inconsistent to compare P/q to mass fluxes at 500 hPa. This discrepancy is in addition to the fact that HS06 did not include the $(1 - RH_{LCL})$ factor, which we find to be crucial in RCEMIP (Figure 7).

Given these issues, the agreement found by HS06 is quite surprising. In Figure B1, we repeated HS06's analysis for the five CMIP6 models in Figure 6a which archived subgrid M_c. We find that the agreement found by HS06 is not robust across models. Notably, MRI-ESM2-0 has an *increase* in 500 hPa subgrid mass flux under warming (in direct contrast to HS06's result), and BCC-CSM2-MR exhibits negligible changes. The other three models exhibit declines in 500 hPa mass flux, but the magnitude of this change does not scale with P/q as closely as in GFDL-CM2.1. Hence, it appears that the original "verification" of Equation 2 by HS06 is likely coincidental.

All-in-all, we suggest that if the reader wants a "rule-of-thumb" for thinking about changes in free-tropospheric M_c with warming it is better to think of mass fluxes as weakening by a few $\%K^{-1}$ in temperature coordinates, rather than following the HS06 scaling.

9. Summary and Conclusions

Our main results are as follows.

- Convective mass fluxes decrease along isotherms with surface warming (Figure 2b). This validates the prediction of J22 across a wide range of cloud-resolving models and GCMs.
- When considered along isotherms, *fractional* changes in M_c become tightly constrained across models, taking on a characteristic value of around 3%–5% K^{-1} (Figure 2c).
- This 3%–5% K^{-1} decline is driven primarily by the stabilization of the tropical lapse rate under warming, and can be captured with a simple analytical model (Figures 3b and 4).
- The HS06 scaling does not robustly capture changes in cloud-base M_c across the RCEMIP models (Figure 7), and their original "verification" was likely coincidental (Appendix B).
- Changes in cloud-base M_c with warming *can* be explained by invoking Betts' Rule (Equation 14), but at the expense of requiring knowledge of (uncertain) changes in cloud-base relative humidity.

It is worth remarking on the historical developments which have led to our theory. In one form of another, it has long been argued that the clear-sky subsidence velocity, w_{sub}, weakens with warming because radiative cooling increases less quickly than atmospheric stability (Held & Soden, 2006; Knutson & Manabe, 1995; Larson et al., 1999). However, the lack of a theory for radiative cooling has prevented this insight from yielding a quantitative constraint. J22 put these arguments on a more secure footing by leveraging the invariance of radiative cooling in temperature coordinates, arguing that w_{sub} (and by mass continuity, M_c) should decrease with warming when plotted in temperature coordinates. In this work, we have validated J22's argument and expanded it into a quantitative constraint on fractional changes in M_c under warming.

We expect this decrease of M_c along isotherms, and its characteristic value of 3%–5% K^{-1}, to be robust, barring large changes in $\alpha(T)$ with warming. But how realistic is this? It appears that there are only minor changes in $\alpha(T)$ in the small-domain RCEMIP simulations we analyzed, but using small computational domains tends to prevent the emergence of convective aggregation and possible changes in aggregation with warming (Wing et al., 2020). Previous work has shown that bulk entrainment rates increase when convection aggregates (Becker et al., 2018), which in concert with a drying of the environment (Muller & Held, 2012) may drive an increase in the re-evaporation of condensate and thus a decrease in α. We have seen hints of such a mechanism occurring in global storm-resolving simulations with a GFDL model and are actively exploring the links between organization, entrainment, α and M_c.

An intriguing result we found was that changes in the "large-scale" M_{up} with warming are tightly constrained across GCMs, and exhibit fractional changes which closely track the lapse-rate contribution (Figures 4c and 4d). This result provides a potential link between thermodynamic changes in the lapse rate and changes in resolved-scale vertical velocities in GCMs, and may provide an alternative explanation for the changes in large-scale tropical circulation under warming. However, it is important to remember that changes in M_{up} can come either from a change in *ascent fraction* or *velocity* (recall that $M_{up} = (-1/g)\sigma_{up}\omega_{up}$). For changes in M_{up} to be linked to changes in the large-scale overturning circulation, they would need to be expressed through ω_{up} and those changes in ω_{up} (defined using daily ω) would need to correspond to changes in the monthly mean ω which are typically used to define tropical circulation strength (e.g., Duffy and O'Gorman (2023)). We are currently investigating these issues.

Another key result of this paper is that the HS06 scaling, although frequently cited in the literature as the physical basis for M_c changes under warming, is a poor model for changes in cloud-base M_c across the RCEMIP ensemble. We have argued that this is primarily because the HS06 scaling assumes that all water vapor lofted into the free-troposphere falls to the surface as precipitation. This assumption can be relaxed by including a $(1 - RH_{LCL})$ factor in the HS06 scaling (as originally proposed by Betts (1998)) which yields a better prediction of changes in cloud-base M_c, but at the expense of requiring knowledge of changes in RH_{LCL} as an input. This drastically limits the usefulness of the HS06 scaling, as changes in cloud-base relative humidity with warming are both large and poorly constrained. We have also offered a critique of the original "verification" of Equation 2 by HS06 and showed it is not robust across GCMs.

While we have shown that the HS06 scaling is not a quantitatively accurate model for changes in M_c under warming, we should emphasize that the key *insight* of HS06 still stands strong. Their essential insight was that radiative cooling (i.e., precipitation) and tropospheric moisture respond differently to warming, and that these two scalings can be combined *without circularity* to constrain the response of mass fluxes to warming. The difference between the changes in moisture and radiation is also crucial to our results. In temperature coordinates, radiative cooling ($-\partial_T F$) is insensitive to surface warming, whereas the "inverse stability" factor still increases with surface warming due to the stabilizing effect of moisture on the lapse rate. That these scale differently with warming is the reason why mass fluxes decline along isotherms with surface warming.

Appendix A: Ambiguity in the Definition of Cloud-Base

A complication when using the HS06 scaling or "Betts' Rule" (Equation 14), which has not been previously emphasized in the literature, is that these constraints apply to mass fluxes at "cloud-base." However, for precipitating cloud fields *there is no single cloud base level*. Instead, the interface between the boundary layer and the free-troposphere is characterized by a broad transition layer over which M_c and RH change rapidly with height (e.g., Malkus (1958) and Figure 1). In the main text we average over the 1–2 km layer to try and capture this transition, but magnitude of changes in cloud-base M_c and RH with warming are quite sensitive to other reasonable definitions of "cloud-base." To illustrate this, in Figures S5 and S6 in Supporting Information S1, we test the sensitivities of the results in Figures 7a and 7b to different cloud-base levels. In these figures we also test the impact of using a weaker vertical velocity threshold in diagnosing M_c. We find that simulated changes in cloud-base M_c are sensitive to these methodological choices. Furthermore, none of these estimates of cloud-base M_c yield values which significantly correlate with the predictions of HS06 (Figure S5 in Supporting Information S1). This ambiguity in the definition of cloud-base adds to the difficulty in using Equation 2 or Equation 14 to understand changes in cloud-base M_c under warming.

Appendix B: Revisiting HS06's Original Result

HS06 "verified" Equation 2 in their paper by comparing fractional changes in global-mean 500 hPa subgrid M_c against fractional changes in global-mean P/q in the GFDL-CM2.1 model. They assumed that q follows Clausius-Clapeyron scaling such that fractional changes in global-mean q can be calculated as $\alpha\Delta T$, where $\alpha = 7\%\mathrm{K}^{-1}$ and ΔT is the change in global-mean temperature.

We reproduce this result in Figure B1a, using their data but without applying a 5-year rolling average to the result (as they do). We also only show the first 150 years of the SRES A1B scenario here, to allow an easier comparison with the CMIP6 models. Their paper does not state how they calculate fractional changes, but we found that we were able to reproduce their Figure 3b by normalizing with respect to the average of the first 5 years of the time series.

We are able to reproduce the equivalence between fractional changes in 500 hPa subgrid M_c and P/q in the CM2.1 model, but is this result robust across models? To our knowledge, no one has ever tested this (note that the validation of "P = Mq" by Vecchi and Soden (2007) uses the same data as HS06).

To test the robustness of HS06's result across models, we applied their methodology to 150 years-long $1\%\mathrm{CO}_2$ runs of the five CMIP6 models we previously used in Figure 6a, this is shown in Figures B1b–B1f. We find that none of these models show such a close correspondence between fractional changes in 500 hPa subgrid M_c and P/q as in the CM2.1 model used by HS06. As noted in the main text, the MRI-ESM2-0 model has an *increase* in M_c at this level, in direct opposition to the result of HS06. Increases in M_c at a given pressure or height level are also found in many of the RCEMIP models (Figure 2a).

These five CMIP6 models were chosen because they archived subgrid M_c and for consistency with the rest of the paper, but we have also assessed this result in a handful of other CMIP5/6 models and found similar results.

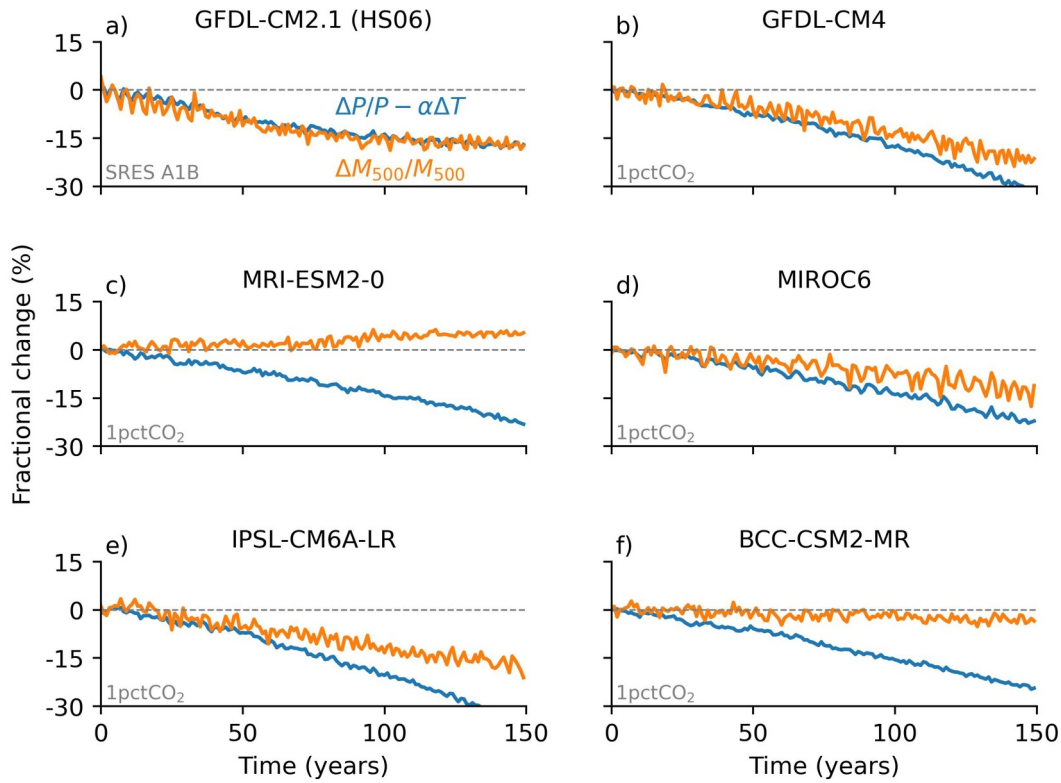

Figure B1. *HS06's original verification of "$P = Mq$" is not robust across GCMs.* Fractional changes in P/q and subgrid M_c at 500 hPa with warming. Changes in q with warming are approximated by $\alpha\Delta T$, where $\alpha = 7\%\text{K}^{-1}$ and ΔT is the global mean temperature change, as in HS06. (a) Is a reproduction of Figure 3b from HS06, using the first 150 years of data from GFDL-CM2.1 under the SRES A1B scenario. (b)–(f) as in panel (a), but for the five CMIP6 models used in Figure 4a. Fractional changes are calculated with respect to the average of the first 5 years of each simulation.

Data Availability Statement

Data supporting the conclusions in this article are archived at Williams (2024). We thank the German Climate Computing Center (DKRZ) for hosting the standardized RCEMIP data, which is publicly available at http://hdl.handle.net/21.14101/d4beee8e-6996-453e-bbd1-ff53b6874c0e.

Acknowledgments
A.I.L. Williams acknowledges funding from the CIMES Postdoctoral Fellowship under award NA18OAR4320123 from the National Oceanic and Atmospheric Administration, U.S. Department of Commerce. We thank Isaac Held, Brian Soden, Ming Zhao, Pu Lin, Tim Merlis, Clare Singer, Sarah Kang, Leo Donner and Hassan Beydoun for helpful discussions, Kris Rand for technical assistance, and Cleo Haussler-Williams for moral support. We also thank three anonymous reviewers for critical comments which improved the clarity and structure of the manuscript.

References

Becker, T., Bretherton, C. S., Hohenegger, C., & Stevens, B. (2018). Estimating bulk entrainment with unaggregated and aggregated convection. *Geophysical Research Letters*, *45*(1), 455–462. https://doi.org/10.1002/2017gl076640

Betts, A. K. (1998). Climate-convection feedbacks: Some further issues. *Climatic Change*, *39*(1), 35–38. https://doi.org/10.1023/a:1005323805826

Bony, S., Stevens, B., Coppin, D., Becker, T., Reed, K. A., Voigt, A., & Medeiros, B. (2016). Thermodynamic control of anvil cloud amount. *Proceedings of the National Academy of Sciences*, *113*(32), 8927–8932. https://doi.org/10.1073/pnas.1601472113

Chadwick, R., Boutle, I., & Martin, G. (2013). Spatial patterns of precipitation change in CMIP5: Why the rich do not get richer in the tropics. *Journal of Climate*, *26*(11), 3803–3822. https://doi.org/10.1175/jcli-d-12-00543.1

Collins, M., Knutti, R., Arblaster, J., Dufresne, J.-L., Fichefet, T., Friedlingstein, P., et al. (2013). Long-term climate change: Projections, commitments and irreversibility.

Duffy, M. L., & O'Gorman, P. A. (2023). Intermodel spread in walker circulation responses linked to spread in moist stability and radiation responses. *Journal of Geophysical Research: Atmospheres*, *128*(1), e2022JD037382. https://doi.org/10.1029/2022jd037382

Grabowski, W. W., Yano, J.-I., & Moncrieff, M. W. (2000). Cloud resolving modeling of tropical circulations driven by large-scale sst gradients. *Journal of the Atmospheric Sciences*, *57*(13), 2022–2040. https://doi.org/10.1175/1520-0469(2000)057<2022:crmotc>2.0.co;2

Hartmann, D. L., & Larson, K. (2002). An important constraint on tropical cloud-climate feedback. *Geophysical Research Letters*, *29*(20), 1951. https://doi.org/10.1029/2002gl015835

He, J., Lu, K., Fosu, B., & Fueglistaler, S. A. (2024). Diverging hydrological sensitivity among tropical basins. *Nature Climate Change*, *14*, 1–6. https://doi.org/10.1038/s41558-024-01982-8

Held, I. M., & Soden, B. J. (2006). Robust responses of the hydrological cycle to global warming. *Journal of Climate*, *19*(21), 5686–5699. https://doi.org/10.1175/jcli3990.1

Held, I. M., Zhao, M., & Wyman, B. (2007). Dynamic radiative–convective equilibria using gcm column physics. *Journal of the Atmospheric Sciences*, *64*(1), 228–238. https://doi.org/10.1175/jas3825.11

Jakob, C., Singh, M., & Jungandreas, L. (2019). Radiative convective equilibrium and organized convection: An observational perspective. *Journal of Geophysical Research: Atmospheres*, *124*(10), 5418–5430. https://doi.org/10.1029/2018jd030092

Jeevanjee, N. (2022). Three rules for the decrease of tropical convection with global warming. *Journal of Advances in Modeling Earth Systems*, *14*(11), e2022MS003285. https://doi.org/10.1029/2022ms003285

Jeevanjee, N., & Romps, D. M. (2018). Mean precipitation change from a deepening troposphere. *Proceedings of the National Academy of Sciences*, *115*(45), 11465–11470. https://doi.org/10.1073/pnas.1720683115

Jenney, A. M., Randall, D. A., & Branson, M. (2020). Understanding the response of tropical ascent to warming using an energy balance framework. *Journal of Advances in Modeling Earth Systems*, *12*(6), e2020MS002056. https://doi.org/10.1029/2020ms002056

Knutson, T. R., & Manabe, S. (1995). Time-mean response over the tropical pacific to increased c02 in a coupled ocean-atmosphere model. *Journal of Climate*, *8*(9), 2181–2199. https://doi.org/10.1175/1520-0442(1995)008<2181:tmrott>2.0.co;2

Koll, D. D., Jeevanjee, N., & Lutsko, N. J. (2023). An analytic model for the clear-sky longwave feedback. *Journal of the Atmospheric Sciences*, *80*(8), 1923–1951. https://doi.org/10.1175/jas-d-22-0178.1

Larson, K., Hartmann, D. L., & Klein, S. A. (1999). The role of clouds, water vapor, circulation, and boundary layer structure in the sensitivity of the tropical climate. *Journal of Climate*, *12*(8), 2359–2374. https://doi.org/10.1175/1520-0442(1999)012<2359:trocwv>2.0.co;2

Liu, J., Yang, J., Ding, F., Chen, G., & Hu, Y. (2024). Hydrologic cycle weakening in hothouse climates. *Science Advances*, *10*(17), eado2515. https://doi.org/10.1126/sciadv.ado2515

Malkus, J. S. (1958). On the structure of the trade wind moist layer.

Malkus, J. S., & Riehl, H. (1964). Cloud structure and distributions over the tropical pacific ocean 1. *Tellus*, *16*(3), 275–287. https://doi.org/10.1111/j.2153-3490.1964.tb00167.x

Manabe, S., & Strickler, R. F. (1964). Thermal equilibrium of the atmosphere with a convective adjustment. *Journal of the Atmospheric Sciences*, *21*(4), 361–385. https://doi.org/10.1175/1520-0469(1964)021<0361:teotaw>2.0.co;2

Mapes, B. E. (2001). Water's two height scales: The moist adiabat and the radiative troposphere. *Quarterly Journal of the Royal Meteorological Society*, *127*(577), 2353–2366. https://doi.org/10.1002/qj.49712757708

McKim, B. A., Jeevanjee, N., Vallis, G. K., & Lewis, N. T. (2024). Water vapor spectroscopy and thermodynamics constrain earth's tropopause temperature. *Authorea Preprints*.

Miyawaki, O., Tan, Z., Shaw, T. A., & Jansen, M. F. (2020). Quantifying key mechanisms that contribute to the deviation of the tropical warming profile from a moist adiabat. *Geophysical Research Letters*, *47*(20), e2020GL089136. https://doi.org/10.1029/2020gl089136

Muller, C. J., & Held, I. M. (2012). Detailed investigation of the self-aggregation of convection in cloud-resolving simulations. *Journal of the Atmospheric Sciences*, *69*(8), 2551–2565. https://doi.org/10.1175/jas-d-11-0257.1

O'Gorman, P., & Muller, C. J. (2010). How closely do changes in surface and column water vapor follow clausius–clapeyron scaling in climate change simulations? *Environmental Research Letters*, *5*(2), 025207. https://doi.org/10.1088/1748-9326/5/2/025207

Romps, D. M. (2014). An analytical model for tropical relative humidity. *Journal of Climate*, *27*(19), 7432–7449. https://doi.org/10.1175/jcli-d-14-00255.1

Romps, D. M. (2016). Clausius–clapeyron scaling of cape from analytical solutions to rce. *Journal of the Atmospheric Sciences*, *73*(9), 3719–3737. https://doi.org/10.1175/jas-d-15-0327.1

Savazzi, A. C., Jakob, C., & Siebesma, A. P. (2021). Convective mass-flux from long term radar reflectivities over Darwin, Australia. *Journal of Geophysical Research: Atmospheres*, *126*(19), e2021JD034910. https://doi.org/10.1029/2021jd034910

Schiro, K. A., Ahmed, F., Giangrande, S. E., & Neelin, J. D. (2018). Goamazon2014/5 campaign points to deep-inflow approach to deep convection across scales. *Proceedings of the National Academy of Sciences*, *115*(18), 4577–4582. https://doi.org/10.1073/pnas.1719842115

Schneider, T., O'Gorman, P. A., & Levine, X. J. (2010). Water vapor and the dynamics of climate changes. *Reviews of Geophysics*, *48*(3). https://doi.org/10.1029/2009rg000302

Seeley, J. T., Jeevanjee, N., & Romps, D. M. (2019). Fat or fitt: Are anvil clouds or the tropopause temperature invariant? *Geophysical Research Letters*, *46*(3), 1842–1850. https://doi.org/10.1029/2018gl080096

Shrestha, S., & Soden, B. J. (2023). Anthropogenic weakening of the atmospheric circulation during the satellite era. *Geophysical Research Letters*, *50*(22), e2023GL104784. https://doi.org/10.1029/2023gl104784

Singh, M. S., & O'Gorman, P. A. (2013). Influence of entrainment on the thermal stratification in simulations of radiative-convective equilibrium. *Geophysical Research Letters*, *40*(16), 4398–4403. https://doi.org/10.1002/grl.50796

Sobel, A. H., Nilsson, J., & Polvani, L. M. (2001). The weak temperature gradient approximation and balanced tropical moisture waves. *Journal of the Atmospheric Sciences*, *58*(23), 3650–3665. https://doi.org/10.1175/1520-0469(2001)058<3650:twtgaa>2.0.co;2

Stauffer, C. L., & Wing, A. A. (2022). Properties, changes, and controls of deep-convecting clouds in radiative-convective equilibrium. *Journal of Advances in Modeling Earth Systems*, *14*(6), e2021MS002917. https://doi.org/10.1029/2021ms002917

Vecchi, G. A., & Soden, B. J. (2007). Global warming and the weakening of the tropical circulation. *Journal of Climate*, *20*(17), 4316–4340. https://doi.org/10.1175/jcli4258.1

Watanabe, M., Iwakiri, T., Dong, Y., & Kang, S. M. (2023). Two competing drivers of the recent walker circulation trend. *Geophysical Research Letters*, *50*(23), e2023GL105332. https://doi.org/10.1029/2023gl105332

Williams, A. (2024). Data for "a robust constraint on the response of convective mass fluxes to warming" [Dataset]. *Zenodo*. https://doi.org/10.5281/zenodo.13694194

Wing, A. A., Reed, K. A., Satoh, M., Stevens, B., Bony, S., & Ohno, T. (2018). Radiative–convective equilibrium model intercomparison project. *Geoscientific Model Development*, *11*(2), 793–813. https://doi.org/10.5194/gmd-11-793-2018

Wing, A. A., Stauffer, C. L., Becker, T., Reed, K. A., Ahn, M.-S., Arnold, N. P., et al. (2020). Clouds and convective self-aggregation in a multimodel ensemble of radiative-convective equilibrium simulations. *Journal of Advances in Modeling Earth Systems*, *12*(9), e2020MS002138. https://doi.org/10.1029/2020ms002138

Zhou, W., & Xie, S.-P. (2019). A conceptual spectral plume model for understanding tropical temperature profile and convective updraft velocities. *Journal of the Atmospheric Sciences*, *76*(9), 2801–2814. https://doi.org/10.1175/jas-d-18-0330.1